Dual-Polarized Antenna with Dual-Differential Integrated Feeding for Wideband Full-Duplex Systems

Dual-Polarized Antenna with Dual-Differential Integrated Feeding for Wideband Full-Duplex Systems

Maksim V. Kuznetcov, Symon K. Podilchak, Ariel McDermott, and Mathini Sellathurai

***Abstract*—A new two-port dual-polarized planar antenna with an integrated feeding circuit for in-band full-duplex (IBFD) applications is presented. The antenna consists of four H-shape slots, stacked patches for enhanced bandwidth (BW), and a separate layer of two differential (0° and 180° split) power dividers connected using vertical transmission lines which define the feeding system. The multilayer antenna is well matched from about 2.2 to 2.5 GHz with isolation values from about 40 to 60 dB. When compared to similar IBFD antenna systems, the proposed configuration provides a higher isolation BW (10%) and higher gain (7.8 dBi) whilst adopting a simple feeding network. Also, by using the proposed feeding circuit, the manufactured antenna does not require any external cables and couplers. This simplifies the structure and reduces the amount of cable connections. This allows for other analog-based self-interference reduction schemes for further improvements in the transmit and receive data link. In addition, the proposed antenna design was extended to a 4×1 array. These dual-differential IBFD antenna systems are a good alternative to more conventional full-duplex designs which typically require external coupler-based feeding. In addition, the operating BWs and isolation values offered by these S-band systems can support new data link possibilities for beam steering and future IBFD wireless networks by low-cost antenna and feeding circuit integration.**

***Index Terms*—Dual-polarization, double-differential antenna, full duplex, isolation, simultaneous transmit and receive (STAR).**

I. Introduction

With the many improvements for traditional data transmissions, full-duplex (FD) systems are once again a topic of interest [1], [2]. For example, significant benefits can be observed when considering in-band full-duplex (IBFD) over out-of-band full-duplex (OBFD) due to the ability of single frequency reuse. Also, in comparison to half-duplex (HD), these FD systems offer increased channel capacity, doubling of the spectrum density and lowering of the delay for two-way communications [3], [4]. This is related to the fact that these systems transmit and receive data simultaneously. However, the challenge that arises in achieving efficient FD systems is overcoming the self-interference (SI) [1]. This interference or noise can be more intense than the signal of interest itself. Simply put, SI in a FD system occurs when one antenna is transmitting and receiving at the same time. Basically the receiver picks up both the transmitted signal, as well as the signal intended for reception, which causes interference.

Recent studies have indicated that for reliable two-way communication in FD mode a minimum of 100 to 140 dB of isolation between the transmitter and receiver is required [5], [6], [7]. To reach such levels of SI suppression, the systems are required to employ different antenna and signal processing methodologies to filter unwanted signals at different network stages or layers. This can make FD systems more expensive and challenging for commercial deployment. To date, the SI suppression methods can be divided into three different domains [8]. The first filtering mechanism could be in the digital domain. This cancellation is challenging due to the fact that analog-to-digital converters (ADC) can be filled with a strong SI signal and a low-power desired signal [9]. An example of a digital SI suppression method is using specialized DSP algorithms when the system estimates the SI level and then subtracts the baseband samples [10]. Another approach could be the improvement of the sampling resolution [11]. This digital domain cancellation is limited and usually can achieve around 20 to 40 dB of SI suppression [12].

On the other hand analog domain cancellation provides higher SI suppression, but is limited by the bandwidth (BW) and the associated cost related challenges. The simplest analog solutions typically consist of couplers, attenuators and phase compensator schemes [13]. Robust and expensive systems can consist of fiber Bragg grating (FBG) filtering mechanisms and circulators for wideband applications [14]. Typical values of SI suppression delivered by the analog domain vary from 30 to 70 dB depending on the complexity of the system [1]. Finally, in the antenna domain, high SI suppression levels have been demonstrated while providing cost effective and compact designs such as the simultaneous transmitting and receiving (STAR) antennas [15] and other beam-forming control solutions for MIMO [16]. Following these efforts antenna suppression methods have received considerable attention due to the demonstrated isolation ranges.

An example of such an antenna was presented in [15]. The dual-polarized antenna consisted of four T-shape parasitic elements mounted on a metallic ground plane defining a non-planar structure. The antenna was able to operate from 0.6 to 1.75 GHz with isolation values of 40 dB. The maximum reported realized gain of the antenna for the receiving and transmitting mode was approximately 7 dBi and 6 dBi, respectively. In a similar fashion, a four-port metallic-based antenna was reported in [17] providing an even wider BW operating from 0.8 GHz to 2.7 GHz. Similar to [15] the antenna design in [17] consisted of resonating ring elements with dipole-like arms. The reported maximum realized gain was 7 dBi with inter-port isolation values below 37 dB over the entire operating range. However, due to the complexity of the design, the manufacturing of such an antenna might be challenging. Moreover, the overall antenna size is almost

$1.4\lambda \times 0.9\lambda$ (diameter and height) while also requiring an external feeding system.

One approach for IBFD is by using an external coupler-based antenna feed system as in [18], [19]. Those antenna systems can offer high isolation values and are based on a single- or double-differential signal shift. To obtain such a signal shift, authors typically make use of hybrid couplers were three ports are employed while the remaining port is terminated by a 50-Ω load. However, the majority of the presented antennas, as in [18] and [19], have offered narrow BWs (approx. 2% to 4%) and maximum gains of 4 dBi due to the patch acting as a resonator.

In those papers the authors pointed out that dual-differential feeding systems can offer higher isolation and better cross-polarization in comparison to single-differential feeding. It should also be noted that for those papers [18], [19], one of the couplers was placed externally to the antenna. This makes the double-differential antenna system become more bulky and cumbersome whilst also requiring additional phase-matched cables, matched loads, and the many connector attachments. All this can increase costs and susceptibility to external noise decreasing isolation levels. This is due to the many physical connections and the possible phase mismatches due to the cables.

Another antenna based on these coupler techniques was presented in [20]. The antenna consisted of four resonating patches on the main board and two boards consisting of one quadrature and two hybrid couplers. With this sequential rotation array (SRA) feed system, dual-CP operation with a maximum gain of 10 dBic was achieved with the antenna requiring a set of phase-matching cables. As a result of the design, the antenna was able to reach 40 dB of isolation in a noisy environment, and up to 65 dB in an anechoic chamber while operating from 2.4 to 2.5 GHz. The authors also proposed additional cancellation layers consisting of a variable phase-shifter, a variable attenuator, and a hybrid coupler for further isolation improvement. With this, the system became more bulky and connection dependent.

Following these trends in the need for simple feeding approaches and low-cost systems, we would like to propose an integrated feeding design (see Fig. 1, 2 and 3) with only two dividers within the same antenna system, and no external couplers, which can offer broadband operation while also employing elevated patches. As outlined in Section II, this design approach can simplify the feeding and reduce the number of required cables, while also, eliminating the requirement of external Rat-race couplers or other hybrids (where one port is typically not used and loaded with 50-Ω). Previously, some more narrowband IBFD antennas used two external hybrid couplers [18], [19], and connecting phase-matched cables were required making the system cumbersome, bulky, and involved to measure mainly due to the external feeding requirements.

In comparison to existing FD antennas and supporting circuit systems as found in the literature (see comparisons in Table I and II), our new two-port single-element antenna offers high isolation levels, employs two slot-based internal power dividers for simple double-differential feeding, requires

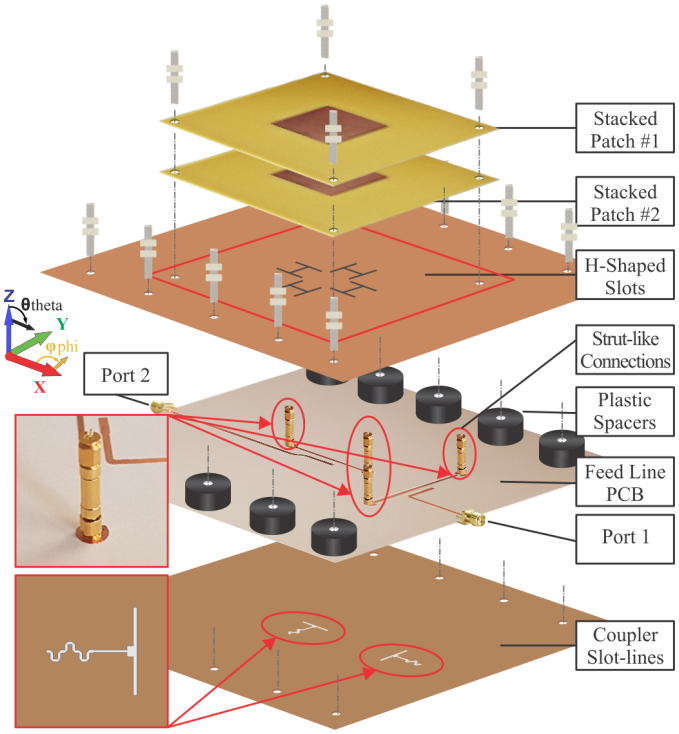

Fig. 1. Antenna design exploded view: 2-port dual-linearly polarized antenna system with H-shaped slots and two parasitic square patch elements on top to increase BW. Bottom differential feeding network consisting of two dividers for 0° and 180° and this signal division circuit is made compact by meandering. Also, vertical strut-like transmission lines connect the multi-layer antenna.

no external cables for antenna operation (i.e cable-less feeding) while also providing a wideband response and low magnitude and phase imbalances for the circuit feeding system. This dual-differential feeding approach is further outlined in Section III while antenna system simulations and measurements are reported in Section IV. In addition, by advancing on this single-element design and the need for higher BW communications and FD beam steering, an extension to 4×1 array is presented in Section V. Some brief conclusions follow in Section VI.

To the best knowledge of the authors, no similar dual-differential antenna element and array have been reported previously whilst offering wideband operation. Basically, by adopting the reported antenna design approaches, the isolation and operating BW can be further enhanced when compared to previous FD antenna systems while maintaining simple cable-less feeding.

II. Single-element Design

The IBFD antenna with the proposed integrated feeding network consists of four H-shaped slots connected to two power dividers, and two patch antennas placed on top of the slot arrangement. The antenna design dimensions are outlined in Fig. 2 and Table III. In particular, the feeding system consists of two slot-line dividers and strut-like vertical connectors for simple manufacturing and assembly. The optimized dimensions for the patch layers and the ground plane are outlined by a through d (see Table III), while the parameters for the H-shaped slots are as follows: e = 0.2 mm, f = 14.6

TABLE I
COMPARISON TO OTHER HIGH ISOLATION ANTENNAS AND ARRAYS FOR FD APPLICATIONS (MEASURED RESULTS UNLESS STATED)

Reference	Frequency	[1]Imped. BW	[2]Isolation Range	Element Size (Lowest Freq.)	Ground Plane (Lowest Freq.)	Height (Lowest Freq.)	Max Gain (Real.)	Boresight Cross-pol.	Circuit Feeding	Feeding Type	Polarization	Antenna Description (Single-element or Array)	Radiation Mechanism & Feeding Configuration
[15]	0.5 to 2 GHz	98%	40 to 55 dB	3.5 by 3.5 λ_0	6 by 6 λ_0	0.2 λ_0	5.5 dBi	<-10 dB	External	-	dual-LP	Non-Planar (Array, 5-port)	Four Dipole-like Elements, Probe Feed
[18]	2.45 to 2.55 GHz	4%	40 to 75 dB	0.22 by 0.22 λ_0	N/A	0.012 λ_0	4.4 dBi	<-24 dB	Integrated	Single-Diff	dual-LP	Planar (Single, 2-port)	Single Rectangular Patch, Microstrip Feed
[19]	2.38 to 2.43 GHz	2%	72 to 98 dB	0.23 by 0.23 λ_0	1 by 0.67 λ_0	0.01 λ_0	4 dBi	<-50 dB	Both	Double-Diff.	dual-LP	Planar (Single, 2-port)	Single Rectangular Patch, Microstrip Feed
[20]	2.4 to 2.5 GHz	3%	50 to 65 dB	0.3 by 0.3 λ_0	1.6 by 1.6 λ_0	N/A	10 dBic	<-24 dB	External	SRA	dual-CP	Planar (Array, 4-port)	Four Rectangular Patches, Probe Feed
[21]	2.3 to 2.7 GHz	20%	37 to 45 dB	0.36 by 0.36 λ_0	N/A	0.13 λ_0	8 dBi	<-16 dB	Integrated	-	dual-LP	Planar (Single, 2-port)	Dipole-like Elements, Probe Feed
[22]	2.4 to 2.5 GHz	4%	41 to 54 dB	0.32 by 0.32 λ_0	2 by 2 λ_0	0.015 λ_0	10.5 dBic	<-15 dB	Integrated	SRA	dual-CP	Planar (Array, 2-port)	Four Rectangular Patches, Microstrip Feed
[23]	4.75 to 5.18 GHz	9%	50 to 58 dB	N/A	3 by 2 λ_0	0.07 λ_0	13.1 dBi	<-24 dB	Integrated	Single-Diff.	dual-LP	Planar (Array, 2-port)	Four Rectangular Patches, Probe Feed
[24]	2.2 to 2.69 GHz	20%	45 to 52 dB	0.55 by 0.55 λ_0	0.7 by 0.7 λ_0	0.2 λ_0	9 dBi	<-30 dB	Integrated	Single-Diff.	dual-LP	Non-Planar (Single, 2-port)	Metallic Probe-like Elements and H-shaped Slot, Loaded Patch
Proposed Antenna	2.25 to 2.48 GHz	10%	46 to 60 dB	0.32 by 0.32 λ_0	1.8 by 1.8 λ_0	0.3 λ_0	7.8 dBi	<-25 dB	Integrated	Double-Diff	dual-LP	Planar (Single, 2-port)	Four H-shaped Slots with Two Loaded Patches
[3]Proposed Array	2.25 to 2.48 GHz	10%	45 to 50 dB	0.32 by 0.32 λ_0	1.8 by 3.4 λ_0	0.3 λ_0	13.3 dBi	<-28 dB	Integrated	Double-Diff	dual-LP	Planar (Array, 8-port)	Sixteen H-shaped Slots with Eight Loaded Patches

[1]The transmit and receive ports -10 dB impedance; i.e. the -10 dB impedance bandwidth (BW) for ports 1 and 2 of the antenna system (or the shared BW).
[2]The corresponding isolation range refers to the external port isolation for the antenna system while the port reflection coefficients are -10 dB (or better).
[3]The developed 4×1 array offers external access to its 8-ports which can easily support beam steering (simulation results described only) and when dual-polarization is required. No similar beam steering features were reported in [15], [18] - [24].

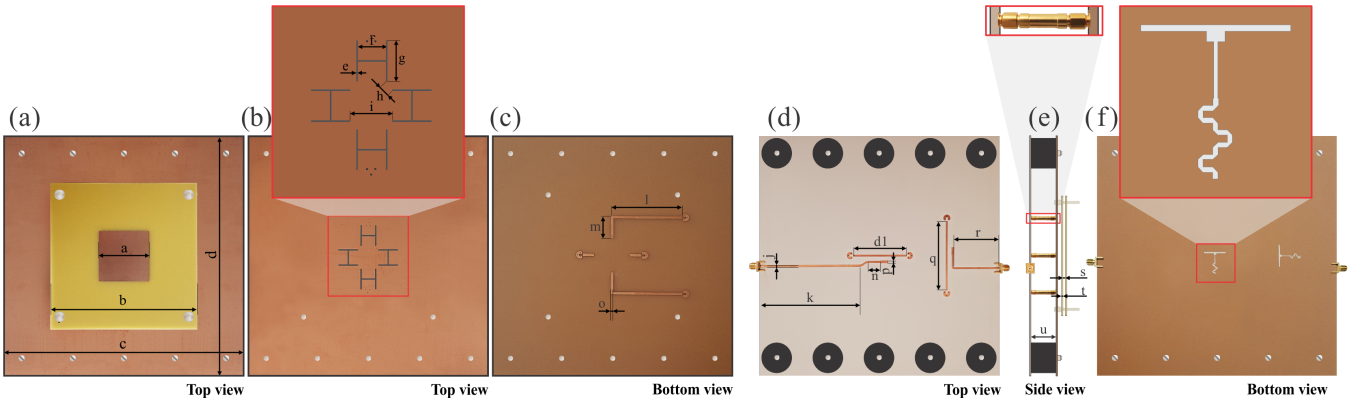

Fig. 2. Antenna design overview. (a) Top view: loaded parasitic patches on top of the H-shaped slots, (b) Top view: four H-shaped slots, (c) Bottom view of the H-shaped board where strut-like connections are positioned for connectivity to the other layers, (d) Top view: feeding system on the second substrate, (e) Side view: strut-like structure connections to the H-shaped slots, (f) Bottom view of the lower substrate; i.e. T-shaped slots of the compact slot-line divider. The dimensions of the antenna and feeding elements can be seen in Table III.

TABLE II
CIRCUIT FEEDING PERFORMANCES (PLANAR) FOR SOME OF THE FD ANTENNAS IN TABLE I

Reference	Frequency Range	[1]Impedance BW (-10 dB)	Phase Imbalance	Mag. Imbalance	Numbers of Power Dividers	Numbers of Hybrid Couplers
[15]	1.15 to 1.65 GHz	35%	<5°	<0.5 dB	-	-
[18]	2.2 to 2.7 GHz	20%	<5°	<0.5 dB	0	1
[19]	2.2 to 2.7 GHz	20%	<5°	<0.5 dB	0	2
[20]	2.2 to 2.7 GHz	20%	<2°	<1.5 dB	0	6
[23]	3.5 to 6.5 GHz	60%	<1°	<0.4 dB	0	1
[24]	1.8 to 3 GHz	50%	<35°	<0.5 dB	1	0
Proposed Antenna	1.85 to 2.8 GHz	40%	<1°	<0.1 dB	2	0
Proposed Array	1.85 to 2.8 GHz	40%	<1°	<0.1 dB	8	0

[1]The -10 dB impedance bandwidth (BW) refers to the percentage frequency BW for which all ports of the feed system offer a -10 dB reflection coefficient (or better).

mm, g = 19 mm, h = 4 mm and the distance between the opposite elements is i = 20.7 mm.

The PCB design material for the patches was FR-4 (see Fig. 1, stacked patch # 1 and # 2) with a relative permittivity of 4.6 and thickness of 1.6 mm. The H-shaped slots serve as an excitation mechanism for the top square patches with the dimensions of b = 48.3 mm for the bottom patch and a = 42.5 mm for the top patch. Other slot-feeding configurations are possible (such as the conventional aperture coupled slot with a length of $\lambda/2$ in the ground plane and with microstrip feeding), but the H-shaped slot can support wideband antenna operation whilst being compact [25], [26]. The optimized distances between patches # 1 and # 2 are t = 9.36 mm, and, defined by s (= 4.16 mm), for the separation between patch # 1 and the H-shaped slots. This multilayer configuration can increase the BW of the antenna system. A single parasitic patch configuration is also possible, but this was shown to reduce the operating BW for the antenna design (all results not reported for brevity).

The overall dimension of the proposed mutli-layer antenna system with four H-shaped slots and two stacked parasitic patches (see Figs. 1 and 2) is c = 240 mm by d = 240 mm (which corresponds to 1.8 by 1.8 λ_0 at the lowest operating frequency of 2.25 GHz). The distance between the H-shaped layer and the feeding layer is u = 24 mm. The relatively large and extended ground plane increases the antenna gain whilst reducing the side lobe levels caused by any parasitic radiation from the the H-shaped slots. The antenna dimensions including the feeding PCB are compiled in Tables III and IV.

III. ANTENNA FEEDING NETWORK

The double-differential integrated feeding network for the antenna consists of two slot-line power dividers. They are designed using compact transmission line meandering considering a Rogers 3003c substrate which has a relative permittivity of 3 and thickness of 0.76 mm. Using this feeding approach the the divider provides dual-differential feeding to the H-shaped slots with a signal shift of 0° and 180°. With this feeding network, two orthogonal linear polarizations are possible for the antenna. For example, by driving Port 1, the generated far-fields in the x-z plane will be linearly polarized (see Fig. 1). Similarly, by exciting Port 2, the dominant fields in the y-z plane will also be linearly polarized. When two dividers have perfect phase balance and the same amplitude, the inter-port leakage of the transmitted and the received signals can be canceled. Thus, the employed slot-line based divider can be utilized for phase and magnitude stability.

The proposed slot-line power divider was designed and simulated in the commercial full-wave simulator CST microwave studio. The design of the divider can be seen in Fig. 3. From

TABLE III
ANTENNA DIMENSIONS AS ILLUSTRATED IN FIG. 2 (ALL VALUES IN MILLIMETERS)

a	b	c	d	e	f	g	h	i	j	k	l	m	n	p	q	r	s	t	u
42.5	48.3	240	240	0.2	14.6	19	4	20.7	2.3	98.3	66.3	21.35	11	3.1	69.5	45	4.16	9.36	24

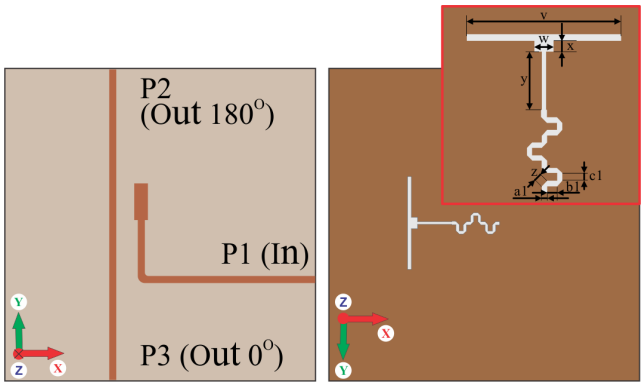

Fig. 3. Top and bottom view for the proposed slot-line divider for the antenna feeding in Fig. 1. The slot-line divider dimensions are outlined in Table IV.

TABLE IV
SLOT-LINE DIVIDER DIMENSIONS AS ILLUSTRATED IN FIG. 3 (ALL VALUES IN MILLIMETERS)

v	w	x	y	z	$a1$	$b1$	$c1$
22	2.5	1.5	8	1.07	1	1.37	0.76

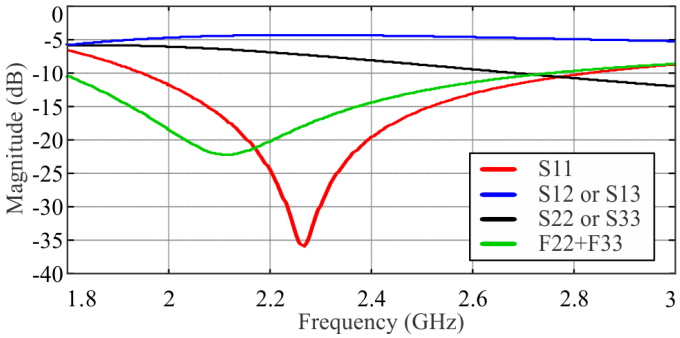

Fig. 4. Simulated S-parameters of the slot-line divider proposed in Fig. 3. Port 1 provides a differential phase shift of 180° between ports 2 and ports 3. When analyzing such a structure, ports 2 and 3 operate considering a differential single shift. Therefore, S22 and S33 are only matched below -5 dB when studying conventional S-parameters. However, when the differential mode is properly considered (or active ports F22 + F33; i.e. when a differential phase is applied at ports 2 and 3) the active matching is well below -10 dB.

the simulations it can be observed that port 1 is well matched from 1.8 to 2.8 GHz with values below -10 dB with a center frequency at 2.28 GHz (see Fig. 4). Due to the employed symmetry, ports 2 and 3 can provide an equal power split ratio with values of -3.5 dB. However, it should be mentioned that ports 2 and 3 are not well matched to 50-Ω and only reach -6 dB (for when 0° phase shifts are applied to both ports). At first glance, it may seem that ports 2 and 3 are not well matched over frequency. However, both ports need to be analyzed together; i.e. ports 2 and 3 operate simultaneously. For this, the divider is required to be analyzed using active S-parameters (or active F-parameters in the CST). In particular, by applying signals to ports 2 and 3 with 0° and 180° phase offsets, the matching is improved and the active F-parameter is below -10 dB over the entire simulated range from about 1.8 GHz to 2.7 GHz. These results suggest that this divider is suitable for the proposed antenna system when port 1 of the slot-line divider circuit (see Fig. 3) is used as the transmitting port.

It should also be noted that in comparison to the conventional Rat-race hybrid coupler, the slot-line power divider magnitude and phase imbalance is much lower. The comparison between a Rat-race coupler with a center frequency of 2.3 GHz and the proposed slot-line divider as well as a Wilkinson power divider (and delay line as in [24]) can can be seen in Fig. 5. The stability of the developed slot-line power divider is wideband over frequency, while the conventional Rat-race coupler and Wilkinson power divider can only provide stability at the center frequency. The full dimensions of the developed slot-type divider are also outlined in Table IV.

IV. INTEGRATION OF THE ANTENNA WITH THE FEEDING SYSTEM & RESULTS

The dividers were further integrated with the single antenna unit as depicted in Fig. 1. It should be mentioned that the integration of both dividers provides simplicity in the feeding system for the multi-layer antenna where only two ports are employed. Also, external couplers are not required. More importantly, this feeding system does not require additional cable connections between the elements whilst employing the strut-like connections. In comparison to more conventional feeding approaches [18]–[20], practical (and unavoidable) cable bending and twisting, as well as the cable connections themselves, could introduce additional phase and magnitude imbalances when external hybrid couplers are needed. This could introduce unwanted main beam tilting issues in the far-field whilst reducing cross-polarization performances. Additionally, the employed slot-line coupler maintains stable magnitude and phase imbalances when compared to the conventional Rat-race couplers (see Fig. 5). Moreover, 50-Ω load terminations at the unused ports are not required as in [18]–[20].

The final antenna design was optimized in CST microwave studio (see results in Fig 6). The antenna is well matched with a simulated -10 dB impedance BW from 2.25 GHz to 2.48 GHz. Due to the employed feeding system, the matching is non-symmetrical, but still offers a significant impedance matching BW which is above 10%. The minimum simulated coupling (S21) is around 2.23 GHz with a value of -54 dB and maximum coupling occurs at 2.42 GHz with the value of -48 dB.

The simulated beam patterns for the Phi = 0° and Phi = 90° planes are presented in Figs. 8 and 9 for ports 1 and 2,

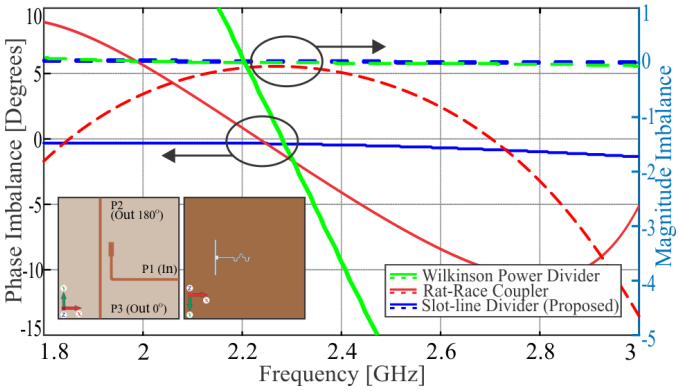

Fig. 5. Simulated phase and magnitude imbalance comparison: Wilkinson power divider with delay line (as in [24]), conventional Rat-race hybrid coupler, and slot-line divider (see inset). It can be seen that the slot-line divider offers a 0.5° phase imbalance or less from 1.8 to 2.5 GHz and can approach 1.2° at 3 GHz (which is out of band of the antenna). Also, maximum magnitude imbalances are around 0.1 dB or less.

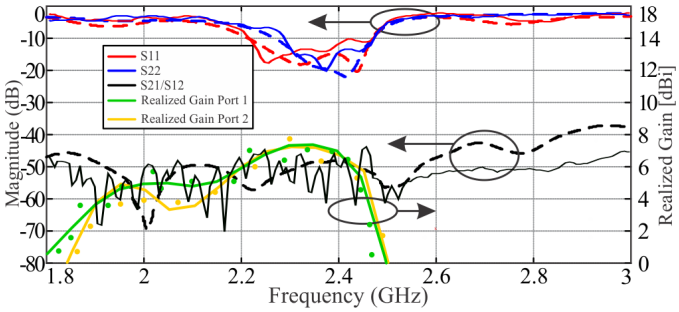

Fig. 6. Simulated (dash line) and measured (solid line) S-parameters of the proposed integrated antenna design. The antenna is well matched from 2.25 to 2.48 GHz (-10 dB BW) while the coupling values are below -50 dB over this BW. The simulated (solid line) and measured (dots) realized gains of the antenna demonstrate a maximum of 7.8 dBi.

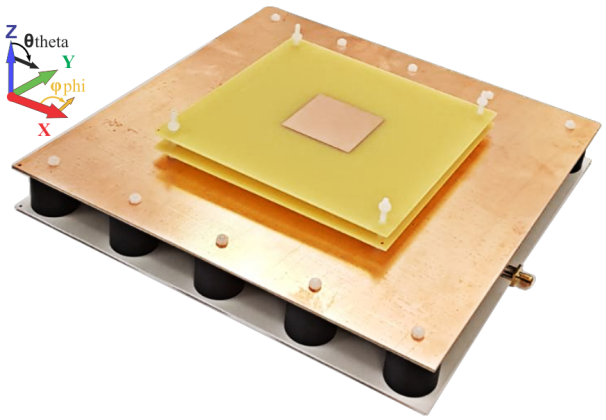

Fig. 7. Manufactured and assembled antenna prototype. The antenna design overview can be seen in Figs. 1 and 2 with full dimensions in the Table III.

respectively. As expected, the antenna is radiating at broadside with cross-polarization values well below 30 dB from the main beam maximum. Maximum realized gain for both ports is 7.8 dBi with port 1 having slightly higher values by about 0.2 dBi at 2.25 GHz (see Fig. 6).

Based on these findings, the proposed IBFD antenna with an integrated feeding system was manufactured and measured. The strut-like connections; i.e. the vertical transmission lines were realized using [27] from Cinch Connectivity while the transitions to microstrip were done using [28] from Amphenol. A photograph of the assembled unit can be seen in Fig. 7. Nylon screws were used to enhance the stability of the structure, provide spacing between the elements, while also reducing any interference between PCBs.

The S-parameter measurements were completed using Keysight PNAs N5225A and 5234A at the Heriot-Watt University Microwave Lab. From the measurements of the S-parameters (see Fig. 6) it can be observed that the coupling, S21, between ports is below -45 dB which is slightly higher than expected when compared to the simulations. The antenna ports are also well matched from 2.25 to 2.49 GHz with values below -10 dB. The slight discrepancy in the isolation is most likely related to a small alignment of the patches on top from the H-shaped structure. It can also be observed that the matching for both ports is not exactly the same. This is related to a needed and minor asymmetry in the feed system (see Fig. 2(d)) and the fact that vertical strut like connections were employed. Also, due to the minor back radiation from the H-shaped slots, the feedline PCB (see Fig. 1) is required to be positioned away from the H-shaped slot PCB layer by the distance u (see Table III). Many optimizations in CST were carried out, however, because of the above noted design requirements, it was challenging to make the reflection coefficients for each port exactly the same as observed in the simulations and measurements while also achieving high levels of isolation.

The DAMS 7100 Diamond Engineering system was used for beam pattern measurements. The reference horn antenna (Flann Horn Antenna Type 08240) was employed. In Figs. 8 and 9 it can be observed that the simulated and measured beam patterns are in agreement. However, the cross-polarization values are higher than expected by about 5 to 10 dB depending on the frequency. This is most likely related to some interactions with the metallic and plastic parts of the antenna positioner.

To compare the developed IBFD single-element with existing antennas and feed systems found in the literature (see Table I and II), it can be observed that the proposed is the only planar antenna system that can offer an improved BW (10%), is fully integrated with its feed system (and double-differential), while also, offering sustained isolation with values reaching 60 dB. In addition, the structure does not require external hybrid couplers or external cables to achieve such isolation levels as in [18]–[20]. These comparisons suggest that the proposed antenna is suitable for IBFD applications whilst providing a simple design approach with integrated feeding. Moreover, this feeding system has been realized with a reduced number of planar circuit elements as well as minimal magnitude and phase imbalances, and, has been demonstrated over a wide impedance BW.

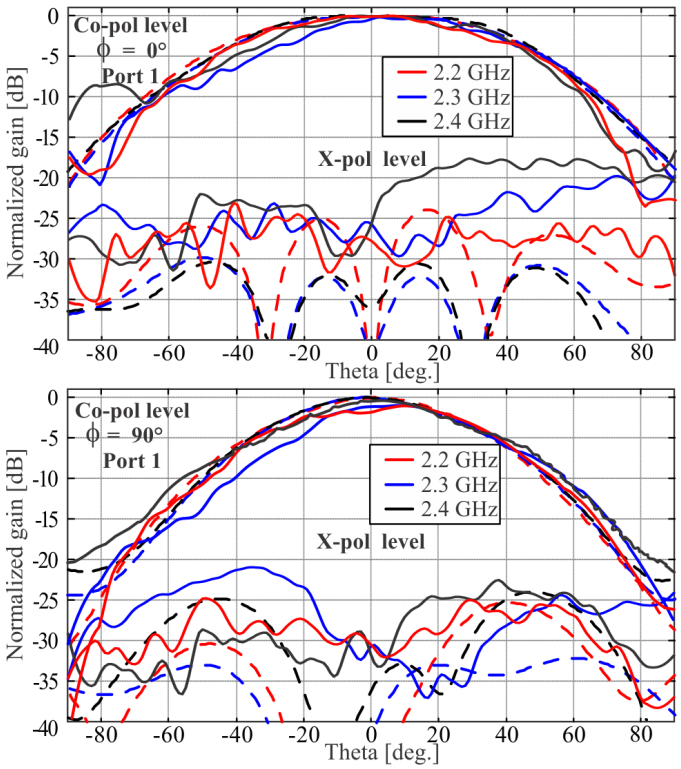

Fig. 8. Simulated (dashed line) and measured (solid line) normalized beam patterns for port 1 at the operating frequencies for the antenna. The cross-polarization levels are below 25 dB at broadside.

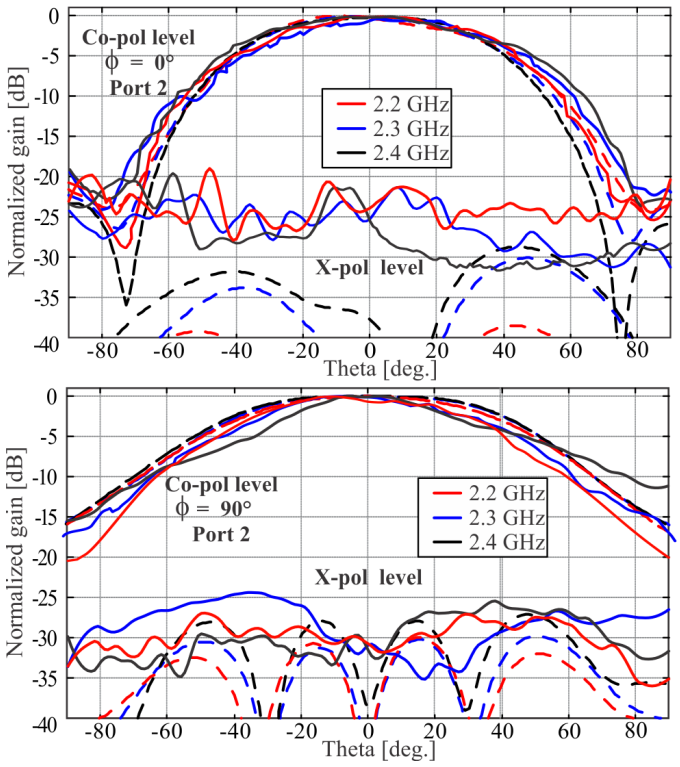

Fig. 9. Simulated (dashed line) and measured (solid line) normalized beam patterns for port 2 at the operating frequencies for the antenna. The cross-polarization levels are below 20 dB at broadside.

V. Full-Duplex 4×1 Array

The proposed IBFD single-element can be well adapted for array applications. Due to the employed integrated feeding system design, we next study a 4×1 array (see Fig. 10). The distance between the radiating elements (patches) is $e1$ = 84 mm (0.67 λ_0 at 2.4 GHz) and the extended ground plane has a total size of $d1$ (= 240 mm) by $f1$ (= 452 mm). Similarly to the single element, the antenna array employs 8 integrated power dividers realizing an 8-port feeding approach.

When designing the FD array, it is important to maintain high port-to-port isolation. From the S-parameter simulations in Fig. 11 of the co-polar elements which generate the same polarization (defining connections to ports 1, 3, 5, and 7), the maximum coupling is about -25 dB or lower (see S13, S15, S17). For the cross-coupling elements (i.e S12, S14, S16 and S18) the highest coupling is between port 1 to port 4 with a value of -42 dB at 2.25 GHz.

The normalized beam patterns for the array can be seen in Figs. 13 and 14. The cross-polarization values are below 30 dB. Similarly to the single element, the antenna is radiating at broadside. The side-lobe levels in the Phi = 90° plane are 12 dB below the main beam maximum. However, due to the presence of the strut-like connectors near the antenna elements of P2 and P8 (for example) and the aforementioned asymmetry in the feeding system for each element as well as the back radiation of the H-shaped slots, the matching is no longer consistent over frequency. Similarly, this can also be observed in the simulations of the array when ideal couplers

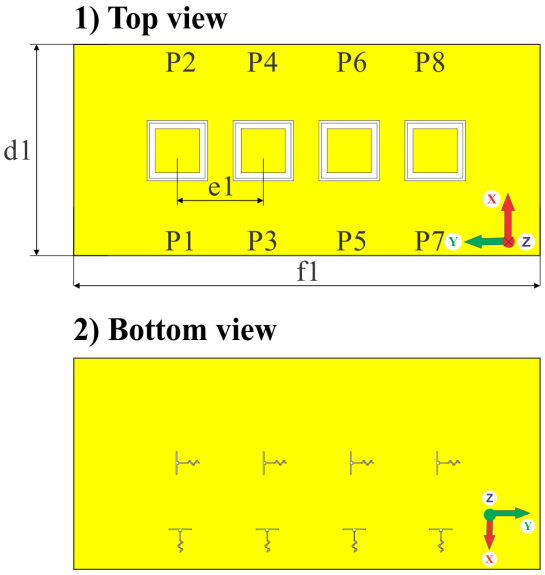

Fig. 10. Top and bottom view of the proposed 4×1 FD array. The system consists of 4 elements with 2 ports for each element for transmitting and receiving defining 8-ports in total for the array. Here ports 1, 3, 5, and 7 are related to the horizontal and linearly polarized far-fields, while ports 2, 4, 6, and 8 define the other polarization.

are considered (see Fig. 12). It should also be mentioned that when the array was simulated without the external feed system and the many strut-like connectors, the maximum realized gain was about 13 dBi for both polarization states.

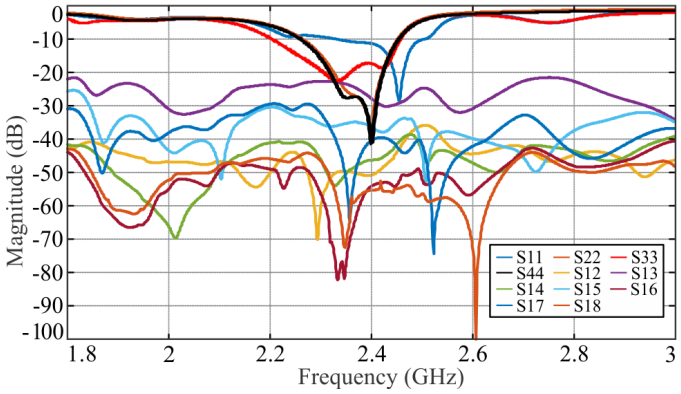

Fig. 11. Simulated S-parameters for the 4×1 FD antenna array as in Fig. 10. It can be seen that the isolation levels are more than 45 dB (see S12, S14, S16, S18) which is similar to the response of the single-element. Maximum coupling within the array is about -25 dB or better (see S13, for example) for the elements which generate the same polarization.

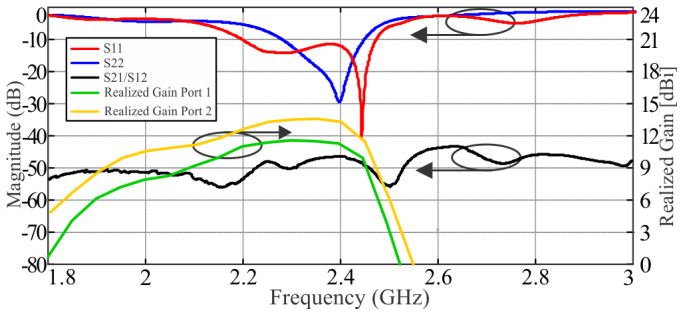

Fig. 12. Simulated S-parameters and realized gain response of the 4×1 FD antenna array considering an external network of 6 ideal power dividers defining feeding points 1 and 2. It can be seen that the isolation levels are below -45 dB which is similar to the single antenna unit (see Fig. 6).

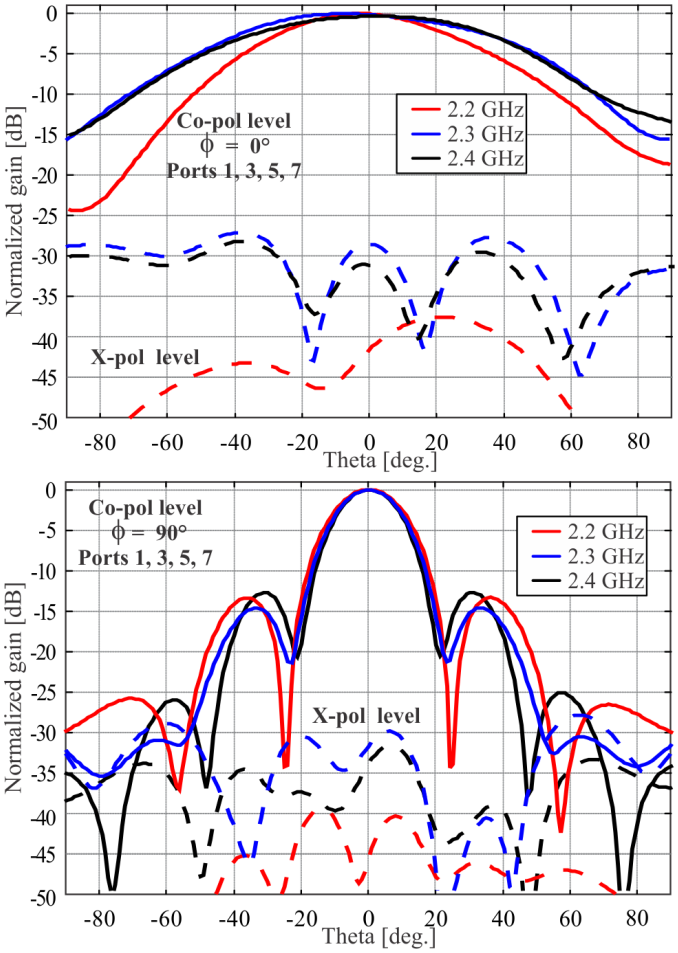

Fig. 13. Simulated normalized beam patterns when driving ports 1, 3, 5, and 7 for broadside radiation at the operating frequencies of the 4×1 array. The cross-polarization levels are below 30 dB at broadside.

Using progressive phase shifts applied to the ports, the simulated antenna array beam steering capabilities are summarized in Tables V and VI with beam patterns in Figs. 15 and 16. It can be seen that the antenna array is capable of beam steering to 32° for both ports with side-lobe levels 7 dB below, or better, from the main beam maximum (which is related to the element spacing of $0.67\lambda_0$ at 2.4 GHz). As described previously elements, ports 1,3,5,7 are for linearly polarized radiation in the x-z plane and ports 2,4,6,8 are for the orthogonal polarization. Basically, for the array, ports 1,3,5,7 (or 2,4,6,8) can work together to excite the elements and generate the far-field beam patterns which can be steered. When considering array feeding with ideal power dividers for system, as further described in Fig. 12, the isolation is well below 45 dB which is similar for the single-element (see Fig. 6). With those considerations, the isolation between the orthogonal polarizations is well below 45 dB.

VI. Conclusion

A dual-linearly polarized antenna and 4×1 array, both with an integrated feeding network, for FD systems was reported. To summarize, the multilayer antenna consists of four H-shaped slots connected to two slot-line power dividers and two patch antennas placed on top of the slot arrangement. The antenna operates from about 2.2 GHz to 2.5 GHz with reflection coefficients below -10 dB. Maximum realized gain for the transmit and receive ports was 7.8 dBi, for the single-element, with isolation values approaching 60 dB.

As described in Tables I and II, the newly reported designs are the only ones which realize double-differential feeding, are fully integrated with the antenna systems, provide wideband operation, and also, achieve the greatest levels of isolation as well as minimal magnitude and phase imbalances for the planar feeding system. Most importantly, the antenna system does not require external hybrid couplers and the many supporting cable connections, etc. which define the more conventional feeding approach [18]–[20] to achieve similar design goals. In addition, the dual-polarized 4×1 array offers external access to its 8-ports. This can support FD beam steering scenarios and by the inclusion of phase shifters or some other beam steering mechanism as required. To the best knowledge of the authors, no similar dual-differential FD array with multiple external ports has been reported (see Table I). Given the developed feeding approach, the antenna systems can also more easily support other isolation enhancement

TABLE V
FULL-DUPLEX ANTENNA ARRAY CHARACTERISTICS CONSIDERING DIFFERENT STEERED BEAM POSITIONS IN THE y-z PLANE FOR PORTS 1, 3, 5, 7

	2.2 GHz				2.3 GHz				2.4 GHz			
Applied Phase	Beam Position	Max. Realized Gain (dBi)	SLL (dB)	Cross-pol. below Beam Max (dB)	Beam Position	Max. Realized Gain (dBi)	SLL (dB)	Cross-pol. below Beam Max (dB)	Beam Position	Max. Realized Gain (dBi)	SLL (dB)	Cross-pol. below Beam Max (dB)
0°	0°	11	-16.3	-38	0°	11.4	-14.7	-31.4	0°	11.2	-12.8	-34
30°	7°	11	-15.3	-30	7°	11.4	-14.7	-30	7°	11.2	-13.1	-30
60°	13°	10.5	-12.7	-28	13°	11.4	-12.1	-31	13°	11.1	-10.5	-27
90°	21°	10	-11.3	-27.9	21°	10.5	-10.7	-31.5	20°	10.7	-9.2	-25
120°	27°	9.4	-11	-29.4	27°	10.3	-12.2	-38	27°	10.7	-9.7	-20.4
135°	29°	8.5	-8.9	-25.8	29°	9.7	-10.4	-42	30°	10.4	-7.7	-24.4

TABLE VI
FULL-DUPLEX ANTENNA ARRAY CHARACTERISTICS CONSIDERING DIFFERENT STEERED BEAM POSITIONS IN THE y-z PLANE FOR PORTS 2, 4, 6, 8

	2.2 GHz				2.3 GHz				2.4 GHz			
Applied Phase	Beam Position	Max. Realized Gain (dBi)	SLL (dB)	Cross-pol. below Beam Max (dB)	Beam Position	Max. Realized Gain (dBi)	SLL (dB)	Cross-pol. below Beam Max (dB)	Beam Position	Max. Realized Gain (dBi)	SLL (dB)	Cross-pol. below Beam Max (dB)
0°	0°	12.3	-13.3	-45.6	0°	13.1	-13	-53	0°	13	-12.1	-51
30°	8°	12.3	-12.8	-42.3	8°	13.1	-10.9	-45	7°	13	-10.9	-50
60°	15°	12.2	-12.3	-36.2	15°	13.1	-10.4	-39	14°	12.9	-10.8	-39
90°	22°	11.8	-11.4	-34	21°	13.1	-10.6	-37	21°	12.8	-10.8	-36
120°	30°	10.9	-10	-36	28°	12.6	-9.4	-51	27°	12	-7.5	-35
135°	34°	10.45	-7.7	-35.2	32°	9.7	-10.4	-49	31°	12	-5	-37

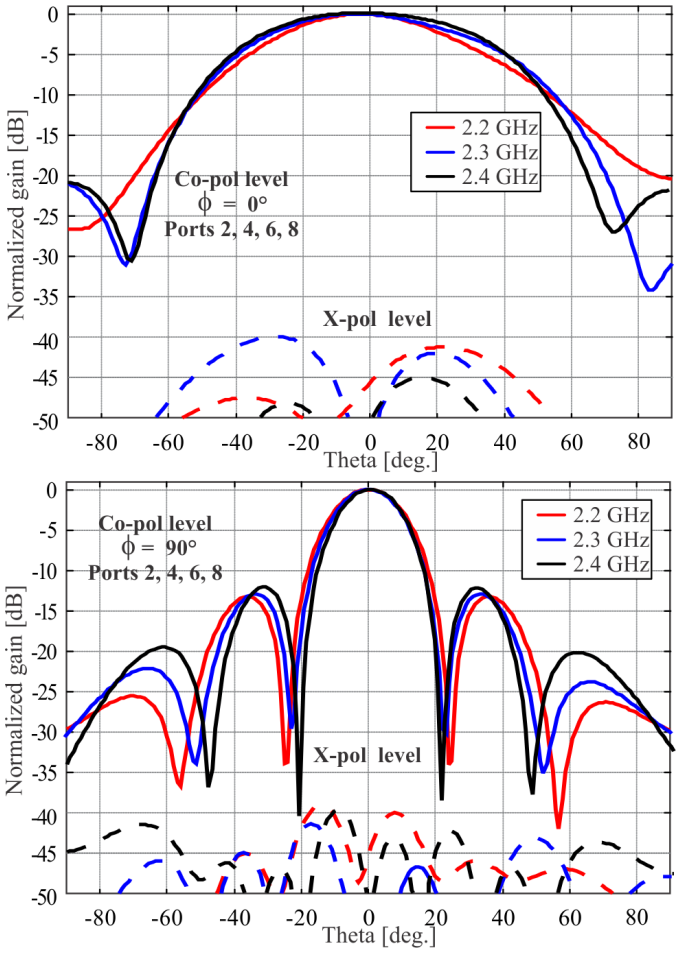

Fig. 14. Simulated normalized beam patterns when driving ports 2, 4, 6, and 8 for broadside radiation at the operating frequencies of the 4×1 array. The cross-polarization levels are below 30 dB at broadside.

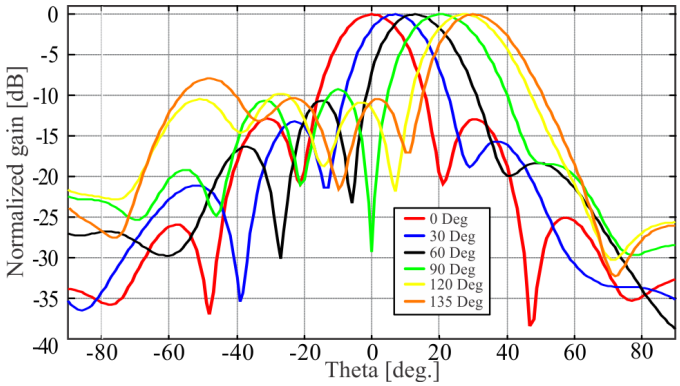

Fig. 15. Simulated beam steering capabilities at 2.4 GHz whilst driving ports 1, 3, 5, and 7 for the 4×1 array using the considered phase shift definitions as in Table V.

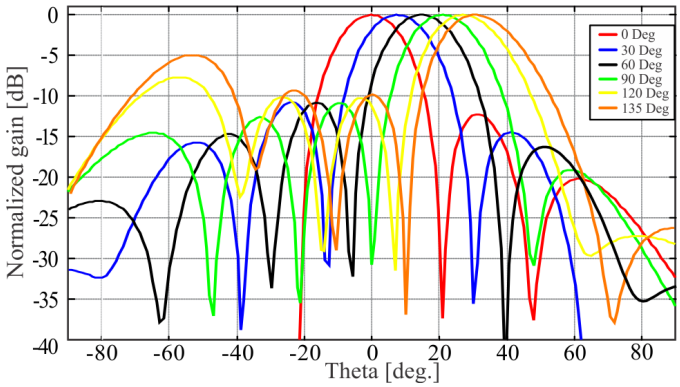

Fig. 16. Simulated beam steering capability in the y-z plane at 2.4 GHz whilst driving ports 2, 4, 6, and 8 for the 4×1 array using the considered phase shift definitions as in Table VI.

schemes which are analog-based. This can further enhance FD operation whilst suppressing the unwanted interference

between the transmitting and receiving signal paths.

REFERENCES

[1] A. Sabharwal, P. Schniter, D. Guo, D. W. Bliss, S. Rangarajan, and R. Wichman, "In-Band Full-Duplex Wireless: Challenges and Opportunities," *IEEE Journal on Selected Areas in Communications*, vol. 32, no. 9, pp. 1637–1652, 2014.

[2] M. Steer, *Microwave and RF Design, Volume 1: Radio Systems*, ser. Microwave and RF Design. University of North Carolina Press, 2019.

[3] Y. Choi and H. Shirani-Mehr, "Simultaneous Transmission and Reception: Algorithm, Design and System Level Performance," *IEEE Transactions on Wireless Communications*, vol. 12, no. 12, pp. 5992–6010, 2013.

[4] G. Liu, F. R. Yu, H. Ji, V. C. M. Leung, and X. Li, "In-Band Full-Duplex Relaying: A Survey, Research Issues and Challenges," *IEEE Communications Surveys Tutorials*, vol. 17, no. 2, pp. 500–524, 2015.

[5] D. Bharadia, E. Mcmilin, and S. Katti, "Full duplex radios," 09 2013, pp. 375–386.

[6] S. Hong, J. Brand, J. I. Choi, M. Jain, J. Mehlman, S. Katti, and P. Levis, "Applications of self-interference cancellation in 5G and beyond," *IEEE Communications Magazine*, vol. 52, no. 2, pp. 114–121, 2014.

[7] M. Duarte, C. Dick, and A. Sabharwal, "Experiment-Driven Characterization of Full-Duplex Wireless Systems," *IEEE Transactions on Wireless Communications*, vol. 11, no. 12, pp. 4296–4307, 2012.

[8] J. Zhou and H. Krishnaswamy, "Recent Developments in Fully-Integrated RF Self-Interference Cancellation for Frequency-Division and Full-Duplex Radios," in *2015 IEEE 81st Vehicular Technology Conference (VTC Spring)*, 2015, pp. 1–5.

[9] D. Korpi, T. Riihonen, V. Syrjl, L. Anttila, M. Valkama, and R. Wichman, "Full-Duplex Transceiver System Calculations: Analysis of ADC and Linearity Challenges," *IEEE Transactions on Wireless Communications*, vol. 13, no. 7, pp. 3821–3836, 2014.

[10] C. A. Schmidt, G. Gonzlez, F. Gregorio, J. E. Cousseau, T. Riihonen, and R. Wichman, "Compensation of ADC-induced distortion in broadband full-duplex transceivers," in *2017 IEEE International Conference on Communications Workshops (ICC Workshops)*, 2017, pp. 1147–1152.

[11] M. Bernhardt, F. Gregorio, J. Cousseau, and T. Riihonen, "Self-interference cancelation through advanced sampling," *IEEE Transactions on Signal Processing*, vol. 66, no. 7, pp. 1721–1733, 2018.

[12] C. D. Nwankwo, L. Zhang, A. Quddus, M. A. Imran, and R. Tafazolli, "A Survey of Self-Interference Management Techniques for Single Frequency Full Duplex Systems," *IEEE Access*, vol. 6, pp. 30 242–30 268, 2018.

[13] B. Debaillie, D. van den Broek, C. Lavn, B. van Liempd, E. A. M. Klumperink, C. Palacios, J. Craninckx, B. Nauta, and A. Prssinen, "Analog/RF Solutions Enabling Compact Full-Duplex Radios," *IEEE Journal on Selected Areas in Communications*, vol. 32, no. 9, pp. 1662–1673, 2014.

[14] K. E. Kolodziej, S. Yegnanarayanan, and B. T. Perry, "Photonic-Enabled RF Canceller for Wideband In-Band Full-Duplex Wireless Systems," *IEEE Transactions on Microwave Theory and Techniques*, vol. 67, no. 5, pp. 2076–2086, 2019.

[15] R. Lian, T. Shih, Y. Yin, and N. Behdad, "A High-Isolation, Ultra-Wideband Simultaneous Transmit and Receive Antenna With Monopole-Like Radiation Characteristics," *Trans. Ant. Prop.*, vol. 66, no. 2, pp. 1002–1007, Feb 2018.

[16] X. Li, T. Jiang, S. Cui, J. An, and Q. Zhang, "Cooperative communications based on rateless network coding in distributed MIMO systems [Coordinated and Distributed MIMO]," *IEEE Wireless Communications*, vol. 17, no. 3, pp. 60–67, 2010.

[17] E. Yetisir, C. Chen, and J. L. Volakis, "Wideband Low Profile Multiport Antenna With Omnidirectional Pattern and High Isolation," *IEEE Transactions on Antennas and Propagation*, vol. 64, no. 9, pp. 3777–3786, Sep. 2016.

[18] H. Nawaz and I. Tekin, "Compact dual-polarised microstrip patch antenna with high interport isolation for 2.5 GHz in-band full-duplex wireless applications," *IET Microwaves, Antennas Propagation*, vol. 11, no. 7, pp. 976–981, 2017.

[19] H. Nawaz and I. Tekin, "Double-Differential-Fed, Dual-Polarized Patch Antenna With 90 dB Interport RF Isolation for a 2.4 GHz In-Band Full-Duplex Transceiver," *IEEE Ant. and Wire. Prop. Lett.*, vol. 17, no. 2, pp. 287–290, Feb 2018.

[20] J. Ha, M. A. Elmansouri, P. Valale Prasannakumar, and D. S. Filipovic, "Monostatic Co-Polarized Full-Duplex Antenna With Left- or Right-Hand Circular Polarization," *Trans. on Ant. and Prop.*, vol. 65, no. 10, pp. 5103–5111, Oct 2017.

[21] L. Sun, Y. Li, Z. Zhang, and Z. Feng, "Compact Co-Horizontally Polarized Full-Duplex Antenna With Omnidirectional Patterns," *IEEE Antennas and Wireless Propagation Letters*, vol. 18, no. 6, pp. 1154–1158, June 2019.

[22] Z. Zhou, Y. Li, J. Hu, Y. He, Z. Zhang, and P. Chen, "Monostatic Copolarized Simultaneous Transmit and Receive (STAR) Antenna by Integrated Single-Layer Design," *IEEE Antennas and Wireless Propagation Letters*, vol. 18, no. 3, pp. 472–476, 2019.

[23] Y. Zhang, S. Zhang, J. Li, and G. F. Pedersen, "A Dual-Polarized Linear Antenna Array With Improved Isolation Using a Slotline-Based 180 Hybrid for Full-Duplex Applications," *IEEE Ant. and Wire. Prop. Lett.*, vol. 18, no. 2, pp. 348–352, 2019.

[24] K. Luo, W.-P. Ding, Y.-J. Hu, and W.-Q. Cao, "Design of dual-feed dualpolarized microstrip antenna with high isolation and low cross polarization," *Progress In Electromagnetics Research Letters*, vol. 36, pp. 31–40, 01 2013.

[25] V. Rathi, G. Kumar, and K. Ray, "Improved Coupling for Aperture Coupled Microstrip Antennas," *IEEE Transactions on Antennas and Propagation*, vol. 44, no. 8, pp. 1196–1198, 1996.

[26] A. Zarreen and S.C.Shrivastava, "An Introduction of Aperture Coupled Microstrip Slot Antenna," *International Journal of Engineering Science and Technology*, vol. 2, 01 2010.

[27] C. C. S. Johnson, "127-0901-811 cinch connectivity solutions johnson: Connectors, interconnects." [Online]. Available: https://www.digikey.com/en/products/detail/cinch-connectivity-solutions-johnson/127-0901-811/1755819

[28] A. S. Microwave, "1211-40001 amphenol sv microwave: Connectors, interconnects." [Online]. Available: https://www.digikey.com/en/products/detail/amphenol-sv-microwave/1211-40001/6050825

Maksim Kuznetcov was born in Kopeysk, Russia, in 1993. He received the M.Eng. degree in electrical and electronic engineering from Heriot-Watt University, Edinburgh, U.K., in 2019. He is currently pursuing the Ph.D. degree with Heriot-Watt University (HWU), Edinburgh, and the University of Edinburgh (UoE), Edinburgh.

In 2019, he joined HWU and UoE as an Research Student, where his research interests include the analysis and design of leaky-wave antennas, duplex and polarization-diverse antenna systems, and other microwave and antenna technologies.

Symon K. Podilchak (S'03-M'05) received the B.A.Sc. degree in engineering science from the University of Toronto, Toronto, ON, Canada, in 2005, and the M.A.Sc. and Ph.D. degrees in electrical engineering from Queens University, Kingston, ON, Canada, in 2008 and 2013, respectively.

From 2013 to 2015, he was an Assistant Professor with Queens University. In 2015, he joined Heriot-Watt University, Edinburgh, U.K., as an Assistant Professor, and became an Associate Professor in 2017. He is currently a Senior Lecturer with the School of Engineering, The University of Edinburgh, Edinburgh, Scotland. His research interests include surface waves, leaky-wave antennas, metasurfaces, UWB antennas, phased arrays, and RF integrated circuits.

He is also a Registered Professional Engineer (P.Eng.) and has had industrial experience as a computer programmer, and has designed 24 and 77 GHz automotive radar systems with Samsung and Magna Electronics. Recent industry experience also includes the design of high frequency surface-wave radar systems, professional software design and implementation for measurements in anechoic chambers for the Canadian Department of National Defence and the SLOWPOKE Nuclear Reactor Facility. He has also designed compact antennas for wideband military communications, highly compact circularly polarized antennas for CubeSats with COM DEV International (now Honeywell Cambridge COM DEV) and The European Space Agency (ESA), and, new wireless power transmission systems for Samsung.

Dr. Podilchak and his students have been the recipient of many best paper awards and scholarships, most notably Research Fellowships from the IEEE Antennas and Propagation Society (AP-S), the IEEE Microwave Theory and Techniques Society (MTT-S), the European Microwave Association, and six Young Scientist Awards from the International Union of Radio Science (URSI). He was also the recipient of the Postgraduate Fellowship from the Natural Sciences and Engineering Research Council of Canada (NSERC). In 2011, 2013 and 2020, Student Paper Awards were received at the IEEE International Symposium on Antennas and Propagation, and in 2012, he was the recipient of the Best Paper Prize for Antenna Design at the European Conference on Antennas and Propagation for his work on CubeSat antennas, and in 2016, the European Microwave Prize for his research on surface waves and leaky-wave antennas. In 2017 and 2019, he was bestowed a Visiting Professorship Award at Sapienza University, Rome, Italy, and from 2016 to 2019, his research was supported by a H2020 Marie Sklodowska-Curie European Research Fellowship. He was recognized as an Outstanding Reviewer of the IEEE TRANSACTIONS ON ANTENNAS AND PROPAGATION, in 2014 and 2020. He was also the Founder and First Chairman of the IEEE AP-S and IEEE MTT-S Joint Chapters in Canada and Scotland, in 2014 and 2019, respectively. In recognition of these services, he was presented with an Outstanding Volunteer Award from IEEE in 2015, and in 2020, MTT-S recognized this Scotland Chapter for its activities and it was awarded the winner of the Outstanding Chapter Award. He has also served as a Lecturer for the European School of Antennas and Associate Editor for the IET Electronics Letters. He is currently a Guest Associate Editor of the IEEE OPEN JOURNAL OF ANTENNAS AND PROPAGATION and IEEE ANTENNAS AND WIRELESS PROPAGATION LETTERS. He was also the recipient of the Outstanding Dissertation Award for his Ph.D.

Ariel J. McDermott was born in Hexham, UK in 1996. He received a Masters degree in Electrical and Electronics Engineering from Heriot-Watt University in Edinburgh, UK in 2019. His primary research area consists of RF, microwave and antenna engineering. He is currently working in the defense industry.

Mathini Sellathurai is currently a Professor of signal processing and wireless communications and Dean of Science and Engineering with Heriot-Watt University, Edinburgh, U.K. She has been active in signal processing research for the past 20 years and has a strong international track record in multiple-input, multiple-output (MIMO) signal processing with applications in radar, and wireless communications. She held visiting positions with Bell-Laboratories, Holmdel, NJ, USA, and at The Canadian Communications Research Centre, Ottawa, Canada. She has published over 200 peer reviewed papers in leading international journals and IEEE conferences, given invited talks and has written several book chapters as well as a research monograph as a lead author. Her present research includes full-duplex systems, passive radar topography, localisation, massive-MIMO, non-orthogonal multiple access, waveform designs, caching technologies, assisted care technologies, IoT, hearing-aids, optimal coded-modulation designs using auto-encoders, channel prediction, and mm-wave imaging and communications. She is a recipient of an IEEE Communication Society Fred W. Ellersick Best Paper Award in 2005, the Industry Canada Public Service Awards for contributions to Science and Technology in 2005, and Awards for contributions to Technology Transfers to Industry in 2004. She was the recipient of the Natural Sciences and Engineering Research Council of Canada (NSERC) Doctoral Award for her Ph.D. dissertation in 2002. She was an Editor for IEEE TRANSACTIONS ON SIGNAL PROCESSING from 2009 to 2014, and from 2015 to 2018, the General Co-Chair of IEEE SPAWC2016 in Edinburgh, and a member for IEEE SPCOM Technical Strategy Committee from 2014 to 2019.